Polyelectrolyte Behavior of Diblock Copolymer Micelles Having Phosphonic Diacid Groups at the Corona

Vanessa Schmidt,[†] Emanuela Di Cola,[‡] Cristiano Giacomelli,[†] Alain R. Brisson,[§] Theyencheri Narayanan,[‡] and Redouane Borsali*,[†,⊥]

Laboratoire de Chimie des Polymères Organiques (LCPO)-ENSCPB−Université Bordeaux 1, 16 Av. Pey Berland, 33607 Pessac Cedex, France; European Synchrotron Radiation Facility (ESRF), BP220, 38043 Grenoble, France; Laboratoire d'Imagerie Moléculaire et Nano-Bio-Technologie (IECB)-Université Bordeaux 1, 2 Rue Robert Escarpit, 33607 Pessac Cedex, France; and Centre de Recherche sur les Macromolécules Végétales (CERMAV, UPR 5301) and Université Joseph Fourier, BP53, 38041, Grenoble Cedex 9, France

Received September 29, 2007; Revised Manuscript Received December 29, 2007

ABSTRACT: The polyelectrolyte behavior of block copolymer micelles originated from the self-assembly of poly(*n*-butyl acrylate)-*block*-poly((1-ethoxycarbonyl)vinylphosphonic diacid) (PBuA-*b*-PECVPD) chains was studied in detail by a combination of potentiometry, static and dynamic light scattering (SLS and DLS), small-angle X-ray scattering (SAXS), and cryo-transmission electron microscopy (cryo-TEM). In aqueous media, the hydrophilic PECVPD micelle corona bearing negatively charged phosphonic diacid groups [$-P(O)(OH)_2$] with two distinct acid dissociation constants conferred interesting pH-, salt-, and concentration-dependent polyelectrolyte features to the system. Light scattering measurements showed the existence of three different regimes in the total scattered intensity (I_{sc}) and apparent hydrodynamic radius (R_H^{app}) vs pH plots, reflecting the influence of the increase in the negative charge density at the micellar corona due to deprotonation. The conformation and interactions of polyelectrolyte chains were more strongly affected by salt addition for solutions with pH $\sim$ 4.0. In such a case, the slope of $KC_p/I(q)$ vs q curves in SLS experiments changed from negative to positive values as the salt concentration (C_s) increased. During this transition, the variation of R_H^{app} measured using DLS put forward the osmotic brush and salted brush regimes, the latter being characterized by a typical $R_H^{app} \propto C_s^{-0.21}$ scaling law. SAXS measurements revealed the core−shell structure and the electrostatic interactions between the micelles which decreased as expected upon the addition of salt. The analysis of the intensity profiles over a wide range of concentrations showed an inhomogeneous core−shell structure with the micelle shell thickness shrinking in presence of added salt. Cryo-TEM images confirmed the spherical shape and narrow size distribution of the micellar nanoparticles.

Introduction

Polyelectrolyte block copolymer micelles originate from the self-assembly of macromolecular chains having, in the simplest AB-type architecture, a sequence of N_A hydrophobic monomers covalently linked to a sequence of N_B charged hydrophilic monomers with an overall composition $f = N_A/N$, where $N = N_A + N_B$. In aqueous environment, the micellar structure comprises a hydrophobic core made from A-blocks segregated from the aqueous exterior and surrounded by a charged hydrophilic shell constituted of B-blocks. When the polyelectrolyte chains are densely tethered to the micelle core surface, they represent the so-called spherical polyelectrolyte brushes (SPB).[1,2] With characteristically complex equilibrium of noncovalent forces (electrostatic, hydrogen bonding, van der Waals, and hydrophobic interactions), SPBs are of great interest in academic research and commercial applications (e.g., surfactants, emulsifiers, flocculants, colloids, rheology modifiers, associative thickeners).[1,3−6]

Light, X-ray, and neutron scattering behavior of charged linear chains, stars, and block copolymer micelles has been the subject of intense research in recent years, and certain features are now reasonably well-established.[7,8] A good summary of the current knowledge of polyelectrolyte solutions with extensive references is given by Förster and Schmidt.[8] Among other parameters such as the solution pH and the degree of dissociation, the ionic strength plays a decisive role in the dimensions and static and dynamic properties of these systems.[2,7−14] For instance, the variation of the brush thickness in a SPB (i.e., the corona width in the case of core−corona micelles) with added salt concentration or grafting density depends on whether the added salt concentration (C_s) is higher or lower than the intrinsic concentration of counterions in the brush ($C_{s,int}$). The two regimes are usually called "salted brush" ($C_s > C_{s,int}$) and "osmotic brush" ($C_s < C_{s,int}$).[5,12] The presence of charges on the polymer chains leads to their expansion with respect to the equivalent neutral counterparts (or highly screened equivalent polyelectrolyte chains), and the lowering in the ionic strength also results in the expansion of polyelectrolyte coils. As the ionic strength decreases, the repulsion between polyelectrolyte chains increases, leading to changes in the second virial coefficient, A_2, and a decrease in the scattering intensity due to osmotic pressure.[1,7,13,14] A feature of polyelectrolytes at concentrations above the overlap concentration (c^*) is the appearance of a scattering peak (or correlation peak) that is frequently observed in X-ray and neutron experiments, while seldom detected using visible light.[13−15]

Synthetic polyelectrolyte block copolymer micelles having poly(acrylic acid) (PAA), poly(methacrylic acid) (PMA), or poly(styrenesulfonic acid) (PSS) as corona-forming blocks are

* Corresponding author. E-mail: borsali@cermav.cnrs.fr.
† LCPO-ENSCPB−Université Bordeaux 1.
‡ ESRF.
§ UBS-IECB-Université Bordeaux 1.
⊥ CERMAV-Université Joseph Fourier.

10.1021/ma702182p CCC: $40.75
Published on Web 02/23/2008

Scheme 1. Chemical Structure and Self-Assembly Behavior in Aqueous Media of the PBuA$_{35}$-*b*-PECVPD$_{30}$ Diblock Copolymer[a]

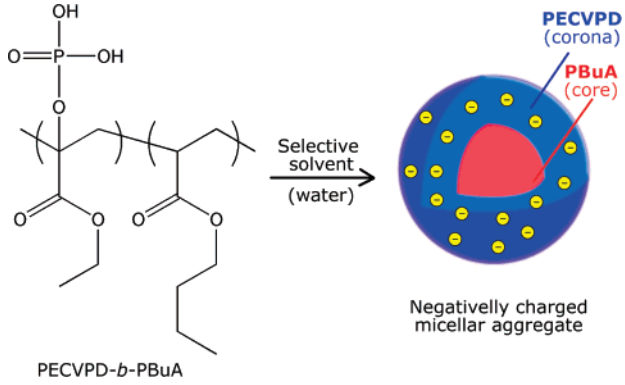

[a] M_n = 11 900 g/mol, M_w/M_n = 1.16, and volume fraction of the PBuA hydrophobic segment ϕ_{PBuA} = 0.43.

the most studied SPB systems, which can in fact be distinguished between two classes: quenched (strongly dissociating chains such as PSS) and annealed (weak polyelectrolyte chains such as PAA and PMA) SPBs.[1,5,8] In the latter case, the number of charges along the hydrophilic segment depends directly on the local pH, which is affected by both the pH and the ionic strength in the bulk of the solution.

The study of polyelectrolyte behavior of charged block copolymer micelles having phosphonic diacid groups at the corona is fundamentally interesting because these moieties have two ionizable protons with distinct dissociation characteristics (one strongly and other weakly dissociating). In the present work, we report on the solution properties of SPBs originated from poly(*n*-butyl acrylate)-*block*-poly((1-ethoxycarbonyl)vinylphosphonic diacid) (PBuA-*b*-PECVPD) copolymers (Scheme 1). Such phosphate-functionalized nanoparticles made from PBuA-*b*-PECVPD are excellent candidates for the design of protein-decorated nanostructures in solution and in bulk.[16,17] They do also exhibit well-defined characteristics of SPB systems, as demonstrated herein mainly on the basis of static and dynamic light scattering (SLS and DLS) and small-angle X-ray scattering (SAXS) experiments.

Experimental Section

Synthesis of the PBuA-*b*-PECVPD Diblock Copolymer. The PBuA-*b*-PECVPD block copolymer was synthesized by atom transfer radical polymerization (ATRP) techniques, as reported by Huang and Matyjaszewski.[18] In the present work, however, a PBuA−Br macroinitiator was used to initiate the controlled radical polymerization of dimethyl(1-ethoxycarbonyl)vinyl phosphate (DECVP) monomer under the following reaction conditions: polymerization in 50% v/v 2-butanone at 70 °C; [DECVP]/[PBuA−Br]/[CuBr]/[1,1,4,7,10,10-hexamethyltriethylenetetramine] = 100/1.0/1.0/1.0. The characteristics of the PBuA$_{35}$-*b*-PDECVP$_{30}$ diblock copolymer (precursor of PBuA$_{35}$-*b*-PECVPD$_{30}$; here and throughout the text, subscripts refer to the mean degree of polymerization (DP) of each segment) are summarized in Table S1 (Supporting Information). Subsequent two-step conversion of −P(O)(OCH$_3$)$_2$ groups into −P(O)(OH)$_2$ phosphonic diacid afforded the mentioned amphiphilic block copolymer.[18]

Preparation of the Aqueous Polymer Solutions. Aqueous PBuA$_{35}$-*b*-PECVPD$_{30}$ copolymer solutions (polymer concentration (C_p) = 0.01−20.0 mg/mL) were prepared by dissolving the appropriate amount of polymer in Millipore water (deionized water, resistance >18 MΩ). The samples were stirred vigorously for at least 2 days at room temperature to allow complete copolymer dissolution and self-assembly. Subsequently, the solutions were filtered using 0.45 μm pore size nylon membrane filters in order to remove dust and large, nonmicellar aggregates. Unless otherwise indicated, the respective ionic strength (I) of each solution was controlled by adding a background electrolyte (NaCl) at a given concentration (C_s). When the block copolymer was dissolved directly in buffered media or at high ionic strength, the formation of large nonmicellar aggregates was observed. Therefore, the aforementioned protocol was applied.

Static (SLS) and Dynamic (DLS) Light Scattering. SLS and DLS measurements were performed using an ALV laser goniometer, which consists of a 22 mW He−Ne linear polarized laser operating at a wavelength (λ) of 632.8 nm and an ALV-5000/EPP multiple τ digital correlator with 125 ns initial sampling time. Data were acquired using ALV Correlator Control software. Copolymer solutions were maintained at a constant temperature of 25.0 ± 0.1 °C in all experiments. The solutions were placed in 10 mm diameter glass cells. The minimum sample volume required for SDLS experiments was 1.0 mL. The accessible scattering angles ranged from 15° to 150° corresponding to wave vectors (q) between 3.45 × 10^{-3} and 2.55 × 10^{-2} nm^{-1}, where $q = (4\pi n/\lambda)\sin(\theta/2)$, θ being the scattering angle and n the refractive index of the solvent (n = 1.33 for water).

SLS measurements were carried out varying the scattering angle (θ) from 40 to 140° with a 5° stepwise increase. Toluene was used as a calibration standard. The variation of $KC_p/I(q)$ was studied as a function of the polymer (C_p) and salt concentration (C_s), where

$$K = 4\pi^2 n^2 (\mathrm{d}n/\mathrm{d}C_p)^2 / N_A \lambda_4 \quad (1)$$

with $\mathrm{d}n/\mathrm{d}C_p$ being the refractive index increment against C_p, N_A is Avogadro's number, and $I(q)$ is the scattered intensity at a given q. The $\mathrm{d}n/\mathrm{d}C_p$ value for PBuA-*b*-PECVPD aqueous micellar solutions is 0.11 mL/g, as determined using a home-built differential refractometer.

DLS experiments were performed using the same ALV apparatus; in this case, the counting time varied from 300 to 900 s. The relaxation time distributions $A(t)$ were in the sequence obtained by CONTIN analysis[19,20] of the autocorrelation function $C(q,t)$. The relaxation frequency, Γ ($\Gamma = \tau^{-1}$), is a function of the scattering angle. The apparent diffusion coefficient (D^{app}) was calculated from the variation of Γ as a function of q through $D = \Gamma/q^2$ at $q \to 0$. The translational diffusion coefficient at infinite dilution (D_0) was then calculated from $D = D_0(1 + k_d C_p)$, where k_d is the concentration virial coefficient. The hydrodynamic radius (R_H) was obtained from the Stokes−Einstein relation $R_H = k_B T/6\pi\eta D$.[19]

Small-Angle X-ray Scattering (SAXS). SAXS measurements were performed at the high brilliance beamline ID02, European Synchrotron Radiation Facility (ESRF), Grenoble, France.[21] A combination of two different sample-to-detector distances was used in order to explore a wide q range, spanning from 0.01 up to 1.0 nm^{-1}, using an incident λ of 0.1 nm, and for X-rays $n \approx 1$.

The SAXS detector was an X-ray image intensifier lens coupled to a fast-readout CCD camera (FReLoN) placed in an evacuated flight tube. Solutions were loaded in a temperature-controlled vacuum flow-through cell (diameter ~2 mm). In addition to the lower background, the sample and solvent scattering can be measured at the same conditions, allowing a very reliable background subtraction.

The normalized background scattering by the capillary filled with the solvent was subtracted from the normalized intensity profiles of the sample, and the resulting quantity is denoted by $I(q)$

$$I(q) = N_p V_p^2 \Delta\rho^2 P(q)\, S(q) \quad (2)$$

where N_p is the number density of scattering particles, V_p is their volume, $\Delta\rho$ is the scattering contrast, $P(q)$ is the form factor describing the shape of the particles, and $S(q)$ is the structure factor describing interparticle interactions. For a relatively dilute suspension, $S(q) \approx 1$ and $I(q)$ is governed by the shape of the scattering objects. In real systems, the scattering objects have a finite size distribution, and the resulting $I(q)$ in the noninteracting case is given by

$$I(q) = N_p \Delta\rho^2 \int_0^\infty V_p^2 P(q,R)\, f(R)\, dR \quad (3)$$

where $f(R)$ can be described using Schulz size distribution function[22]

$$f(R) = \left(\frac{Z+1}{R_m}\right)^{Z+1} \frac{R^Z}{\Gamma(Z+1)} \exp\left(-\frac{Z+1}{R_m} R\right) \quad (4)$$

with $Z = 1/(1-p^2)$, p being the polydispersity and R_m the average size.

$P(q)$ can be expressed in terms of the scattering amplitudes of two spheres of radii (R_c) and ($R_c + t$), where t is the thickness of the shell:

$$V_p^2 \Delta\rho^2 P(q,R) = (16\pi^2/9)\{(\rho_{core} - \rho_{shell}) R_c^3 F(q,R_c) - (\rho_{solvent} - \rho_{shell})(R_c + t)^3 F(q,R_c + t))^2 \quad (5)$$

with $F(qR_i) = 3[\sin(qR_i) - qR_i \cos(qR_i)]/(qR_i)^3$ and $P(q,R_i) = F^2(q,R_i)$. ρ_{core}, ρ_{shell}, and $\rho_{solvent}$ are the scattering length densities of core, shell, and solvent, respectively.

Data were analyzed using the form factor $P(q)$ of spherical core−shell objects, and the best fits of the modeled SAXS functions were derived by using the form and structure factors implemented in BHplot program.[23]

Above the overlap concentration (c^*) the interactions between the particles are not negligible. For simplicity, $S(q)$ is approximated by an effective structure factor of hard spheres system within Perkus−Yevick approximation.[24] In this case the effective volume fraction is given by

$$\varphi = \frac{\pi}{6} N_p \sigma^3 \quad (6)$$

where $\sigma = 2(R_c + t + R_e)$ is the effective diameter taking into account the contribution of hard core, the impenetrable shell, and the range of electrostatic interactions (R_e). In both the cases of solution with and without added salt the particles form permanent clusters which give rise to an excess of scattering in the low-q region. This additional scattering can be described with a Lorentian term $S_c(q)$, corresponding to the structure factor of the clusters[24]

$$S_c(q) = \frac{I_M}{(1 + \xi^2 q^2)^d} \quad (7)$$

where I_M and ξ are proportional to the average mass and characteristic size of the clusters ($\xi^2 \approx R_g^2/3d$) and d is a power law exponent related to the fractal dimension of the clusters ($d \approx d_f/2$).

Thus, the total intensity including the cluster term is given by

$$I(q) = N_p \Delta\rho^2 V_p^2 P(q)[S(q) + S_c(q)] \quad (8)$$

Cryo-Transmission Electron Microscopy (Cryo-TEM). A Leica CPC quench-freezing device was used to prepare cryo-TEM specimens. Drops of sample were deposited on holey carbon grids. After blotting the excess of liquid with filter paper, the grids were immediately plunged into liquid ethane cooled to −170 °C with liquid nitrogen. The grids were mounted on a Gatan 626 cryoholder transferred in to the microscope, and kept at a temperature of about −175 °C. EM was performed with Tecnai-F20 FEI-transmission electron microscope, operating at 200 kV. Low-dose images were recorded at a nominal magnification of 50 000× with 2K × 2K 45C1000 slow-scan CCD camera.

Results and Discussion

Solution Behavior of PBuA-*b*-PECVPD. The PECVPD polymer is formed by monomer units having at the same time two pendant groups with opposite solubility properties. While the ethyl side groups are typically hydrophobic and hence insoluble in water, the presence of an equal number of highly hydrophilic phosphate moieties along the chain ultimately confers temperature responsiveness to system. It has been observed that PDECVP dissolves molecularly in water at low temperature but switches from hydrophilic to hydrophobic at a given critical solubility temperature (CST) upon heating.[18] The characteristic CST of PDECVP depends on both C_p and M_n, decreasing with the increase of such parameters. It was observed, for example, that the CST of a M_n = 14 900 g/mol sample decreases from 85 to 77 °C as the C_p increases from 5.0 to 20.0 mg/mL.[18]

Therefore, at ambient temperature the $PBuA_{35}$-*b*-$PECVPD_{30}$ diblock copolymer consists of two segments of opposite water solubility, water being a solvent thermodynamically good for PECVPD but poor solvent for PBuA. As a result, $PBuA_{35}$-*b*-$PECVPD_{30}$ chains self-assemble upon contact with aqueous environment into spherical micellar aggregates, whose structures comprise a hydrophobic PBuA core and a hydrophilic PECVPD corona bearing negatively charged phosphate moieties (Scheme 1). The critical micelle concentration (cmc) of this system was found to be 0.002 mg/mL in water (no added salt), as determined by fluorescence spectroscopy using pyrene as probe (Supporting Information, Figure S1). This value is fairly comparable with those reported in the literature for poly(butyl acrylate)$_{90}$-*b*-poly(acrylic acid)$_{100}$ ($PBuA_{90}$-*b*-PAA_{100})and poly(*t*-butyl styrene)$_{26}$-*b*-poly(sodium styrenesulfonate)$_{413}$ ($PtBS_{26}$-*b*-$PSSNa_{413}$) SPB systems.[12,25] Interestingly, the relative intensities of the first (F_1 at 372 nm) and the third (F_3 at 383 nm) bands in the pyrene emission spectrum at $C_p \gg$ cmc suggested that the polarity of the hydrophobic microenvironment (core)[26] of $PBuA_{35}$-*b*-$PECVPD_{30}$ micelles ($F_3/F_1 = 0.85$) is even slightly lower than for the $PBuA_{90}$-*b*-PAA_{100} micelles ($F_3/F_1 = 0.71$) with longer hydrophobic segments.

The phosphonic diacid groups at the micelle corona exhibit two ionizable protons with distinct acid dissociation constants (K_a), as also observed for other substituted phosphate compounds containing labile protons. The pK_a (= −log(K_a)) for the first dissociation process is very low (p$K_{a1} \sim 2.0-3.0$), whereas the second deprotonation occurs at nearly neutral pH conditions (p$K_{a2} \sim 5.0-7.0$). Therefore, the titration of $PBuA_{35}$-*b*-$PECVPD_{30}$ solutions can be modeled as follows

$$H_2P \overset{K_{a1}}{\rightleftharpoons} HP^- + H^+ \overset{K_{a2}}{\rightleftharpoons} P^{2-} + 2H^+ \quad (9)$$

where H^+ is the proton (or hydronium ion), H_2P denotes the uncharged (protonated) block copolymer, and HP^- and P^{2-} represent the corresponding chains formed by monomers with one or two negative charges each, respectively.

Potentiometric measurements were performed in order to gain insight into the pH effect on the effective number of charges on the micellar corona. The results (Supporting Information, Figure S2) revealed that the first dissociation process takes place at pH < 3, being therefore not detectable in the titration curve (i.e., pK_{a1} < 3.0). Starting from pH = 3.0, the addition of small aliquots of NaOH increases the solution pH until a slightly pronounced buffering region is reached (shoulder), during which the added NaOH is consumed by the titration of the second proton on the ECVPD repeat units. Further addition of base merely elevates the solution pH. The estimated average pK_{a2} was 6.5. On basis of these results, the diagram of species distribution (Figure S3), and ultimately the variation in the total number of charges at the micelle corona, as a function of the solution pH can be calculated (Figure 1). At pH ≥ 4 at least one permanent negative charge is constantly present on each

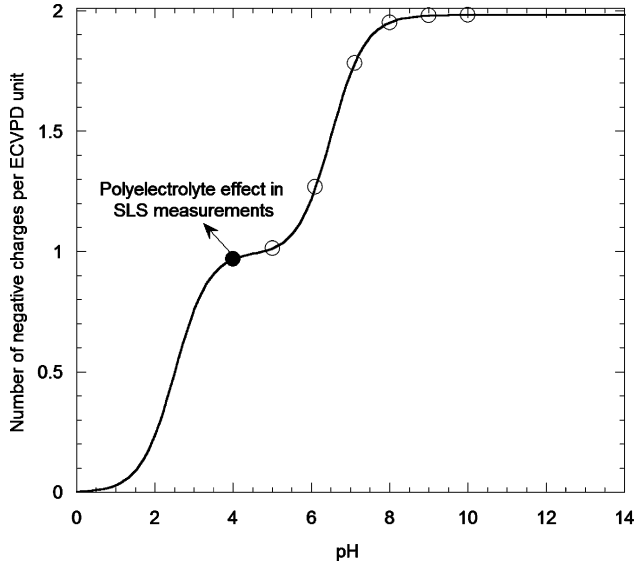

Figure 1. Number of negative charges per ECVPD monomer unit as a function of the solution pH. The circles correspond to pH conditions at which the systems were investigated.

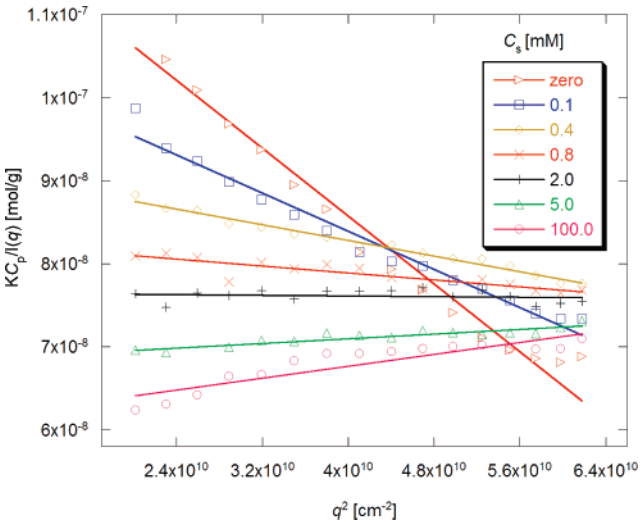

Figure 2. $KC_p/I(C_p,q)$ vs q^2 curves for 0.5 mg/mL $PBuA_{35}$-*b*-$PECVPD_{30}$ micellar solutions containing different amounts of added NaCl salt.

monomer unit of the PECVPD chain (HP^- species), while at pH > 5 the fraction of fully ionized phosphate moieties (P^{2-} species) increases, so that at pH = 7.8 more than 95% of maximum deprotonation extent (dissociation degree) is attained. It is worth noting that such an information is of great relevance for the diblock copolymer nanoparticles herein investigated as far as it precisely defines the experimental conditions where variations in the effective micellar charge occur, for instance doubling from pH = 4.0 to 8.0. Besides, it allows the calculation of the actual number of negative charges per micelle provided that the aggregation number (N_{agg}) is known (see below).

Light Scattering. Figure 2 shows the variation of $KC_p/I(q)$ as a function of q^2 for 0.5 mg/mL micellar solutions containing different amounts of added NaCl salt (C_s = 0−100 mM), as indicated. The characteristic solution pH measured for this sample was ~4.0, not being significantly influenced by C_s. Therefore, under these experimental conditions each monomer of the PECVPD chains has one permanent negative charge (Figure 1), and the particles dispersity is about $\mu_2/\Gamma^2 = 0.15-0.25$, as estimated by cumulants analysis of $C(q,t)$ autocorrelation functions by DLS. In Figure 2, a steeply negative slope

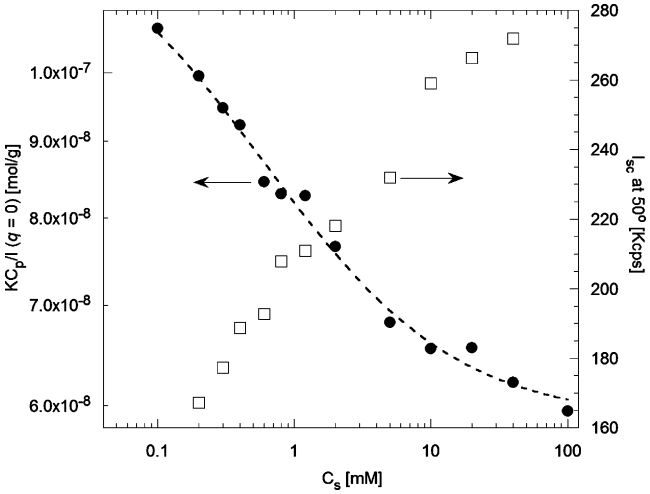

Figure 3. $KC_p/I(C_p,q=0)$ as a function of C_s for 0.5 mg/mL $PBuA_{35}$-*b*-$PECVPD_{30}$ micellar solutions.

was observed in absence of salt, indicating strong interparticle correlations. As C_s increased up to $C_s \leq 0.8$ mM, the slope decreased progressively, then became positive for $C_s > 2.0$ mM, and finally remained increasing slightly as C_s continued to increase. A virtually constant slope was evidenced for $C_s >$ 10−20 mM. At this point, the electrostatic interactions (repulsions) within the micelle corona are presumably shielded by added salt ions,[7,14] so that further addition of salt practically did not affect the micelle structure. Such polyelectrolyte behavior was also confirmed by an abrupt increase in the scattered light intensity (I_{sc}) as a function of C_s (see below), in spite of the fact that micelle dimensions (corona thickness) decreased in presence of salt. The increase in I_{sc} reflected the higher mobility of scattering objects upon screening of electrostatic repulsions by counterions.[1,7,13,14]

Negative slopes in $KC_p/I(q)$ vs q^2 curves were previously observed for linear polyelectrolytes in light scattering experiments.[14,27] However, the results in Figure 2 are considered the first reported evidence for polyelectrolyte block copolymer micellar systems.

Figure 3 describes the variation of the intercept $KC_p/I(q=0)$ as a function of C_s (i.e., the values of $KC_p/I(q)$ at $q = 0$ found from linear extrapolation of data in Figure 2), and the increase in the scattered light intensity (I_{sc}) as a function of C_s. It is worth noting that $KC_p/I(q=0) \cong 1/M_w + 2A_2C_p$ at $q = 0$ (classical Zimm equation). When the latter relation is applied to the $PBuA_{35}$-*b*-$PECVPD_{30}$ micellar system herein investigated, the left-hand side term $1/M_w$ is a constant value as long as after micellization the M_w the micelles ($M_{w,mic}$) is not affected by changes in the ionic strength (see discussion below on SAXS data). Therefore, the decrease in $KC_p/I(q=0)$ observed in Figure 3 essentially reflects the decrease in the second virial coefficient (A_2) and in the radius of gyration (R_g).[14,28] At high salt concentrations, A_2 is reduced by approximately half its initial value. It is possible, therefore, to distinguish the electrostatic portion of the A_2 value from the limiting A_2 value of residual highly screened (or "neutral") micelles. The overall profiles of $KC_p/I(q=0)$ vs C_s curves for $PBuA_{35}$-*b*-$PECVPD_{30}$ micelles and linear sodium hyaluronate are reasonably comparable.[14]

The conformation and interactions of polyelectrolyte chains are strongly influenced by the addition of salt. In the case of SPBs such effects are particularly pronounced as long as the charged chains at the corona are more closely packed. Two regimes with characteristic brush thickness (corona width (W)) behavior can be distinguished for SPBs depending on the ratio

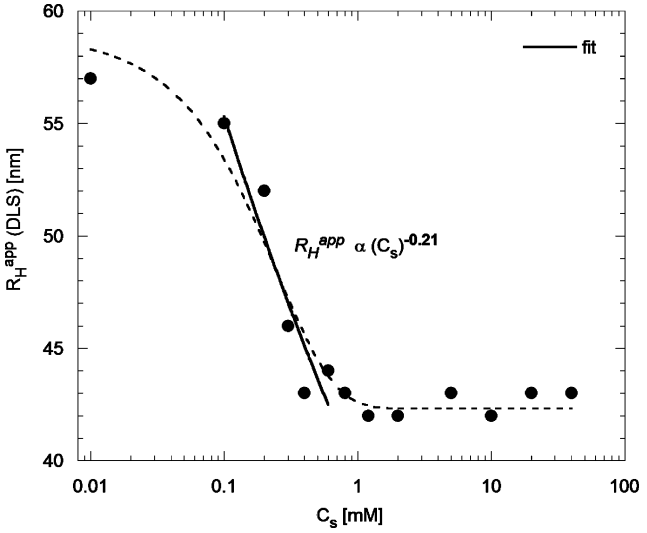

Figure 4. Apparent hydrodynamic radius (R_H^{app}) of $PBuA_{35}$-*b*-$PECVPD_{30}$ micelles as a function of C_s.

between intrinsic brush counterion concentration ($C_{s,intr}$) and the added salt concentration (C_s).[5] In the so-called osmotic brush regime ($C_{s,intr} > C_s$) the changes in C_s have no effect on W, whereas in the salted regime ($C_{s,intr} < C_s$) W usually decreases with the increase in C_s, and this according to a $W \sim C_s^{-\beta}$ scaling law. Korobko et al.[29] have contemplated that the gradual contraction of charged micelles scales as $W \sim C_s^{-1/5}$, whereas other authors reported that a $W \sim C_s^{-1/3}$ dependence should be expected.[1,5,30,31] Experimentally, β values varying from 0.11 to 0.18 have been found for SPBs so far.[31]

The variation of the apparent hydrodynamic radius (R_H^{app}) as a function of C_s for 0.5 mg/mL micellar solutions is shown in Figure 4, where $R_H^{app} = W + R_c$ with R_c being the micelle core radius which is not influenced by the ionic strength (see hereinafter). Therefore, the variation in R_H^{app} as a function of C_s is ascribed to changes in W. In line with findings presented above, the results in Figure 4 also demonstrate that small amounts of salt provoke major changes in the macromolecular chain organization at the micelle corona, as judged from the rapid decreased in R_H^{app} from 57 to 41 nm as C_s increased from 0.1 to 1.0 mM. Further addition of salt did not influence the system. For 0.1 mM $\leq C_s \leq$ 1.0 mM, a $W \sim C_s^{-0.21}$ dependence is observed in Figure 4. This finding is in slightly better agreement with the expected value as compared to earlier reports on, for example, PS-based lattices with polyelectrolyte brushes at the surface ($W \sim C_s^{-0.17}$)[30] and block copolymer micelles made of poly(ethylethylene)$_{144}$-*b*-poly(styrenesulfonic acid)$_{136}$ (PEE_{144}-*b*-$PSSH_{136}$, $W \sim C_s^{-0.13}$)[12] and $PtBS_{27}$-*b*-$PSSNa_{757}$ ($W \sim C_s^{-0.11}$).[32]

As outlined above, the density of negative charges at the micelle corona and consequently the scattering properties of the system depend on the solution pH and the ionic strength. The variation of the total scattered light intensity (I_{sc}) at 90° scattering angle and the number of charges on each ECVPD monomeric unit as a function of the pH are shown in Figure 5. The results reveal the existence of three different regimes in the I_{sc} vs pH plot, as indicated. Initially, (a) the I_{sc} decreases steeply by almost half its initial value as the pH is increased from 4.0 to 6.5 via addition of NaOH. Then, (b) a small decrease is also observed within the pH = 6.5−8.0 range. Finally, (c) the I_{sc} slightly increases for 8.0 < pH < 10.0 solutions.

The overall profile in Figure 5 reflects the increase in the negative charge density at the micellar corona due to the second deprotonation process of phosphonic diacid groups. The enhanced interparticle electrostatic repulsions reduce the mobility of scattering particles, consequently lowering I_{sc} as well (regimes a and b). At pH ≥ 8.0 (regime c) the degree of acid dissociation is nearly quantitative (>97%, Figure 1), and the influence of further addition of a strong base (NaOH) is similar to the salt effect (i.e., I_{sc} increases due to higher mobility of scattering objects upon screening of electrostatic repulsions by counterions). The data in Figure 5 also reveal an interesting feature regarding the transition from regimes a to c. The interception of the linear fittings in those respective regions coincides at pH ∼ pK_{a2}, a point at which the second deprotonation extent is 50%. To the best of our knowledge, such an observation has not been reported yet for weakly dissociating polymer brushes. Most likely, this behavior results from the balance of two opposing forces: the generation of charges at the micellar corona whose effect (I_{sc} decrease) is more pronounced in beginning of the process (i.e., at very low added NaOH concentrations; C_{NaOH} ∼ 2 mM at pH = 6.5) and the inevitable increase in the ionic strength (I_{sc} increase) due to the addition of ionic species ($Na^+_{(aq)}$ and $OH^-_{(aq)}$; the latter is partially consumed during the neutralization reaction).

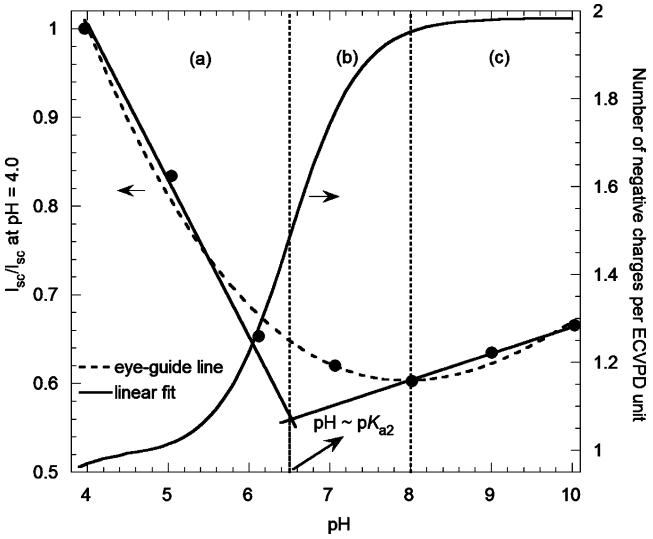

Figure 5. Variation of the total scattered light intensity (I_{sc}) as a function of the solution pH for 0.5 mg/mL $PBuA_{35}$-*b*-$PECVPD_{30}$ micelles.

Small-Angle X-ray Scattering. The morphology and the interactions of negatively charged $PBuA_{35}$-*b*-$PECVPD_{30}$ micelles were investigated by small-angle X-ray scattering (SAXS) experiments carried out at different polymer concentrations (C_p = 0.5−20 mg/mL) and added salt contents (C_s = 0−200 mM). Figure 6 shows a typical SAXS intensity profiles obtained at different C_p without added salt (C_s = 0), as indicated. At a glimpse, different structural levels can be qualitatively observed: in the high-q region the complex internal structure of the micelle is manifested, which provides the micelle core size ($R_c \approx$ 21 nm); for C_p > 2.5 mg/mL at intermediate q, a correlation peak due to micelle−micelle interactions can be observed at $q = q^*$; furthermore, in the low-q region permanent clusters give rise to the upturn in all the scattering patterns.

At high charge and minimal screening conditions, the polyelectrolyte chains remain almost fully stretched and they interdigitate.[29,33] Meanwhile, C_p was found to have practically no influence on the micellar dimensions, as judged from the high-q SAXS data shown in Figure 6. Indeed, the $I(q)$ minima at $q \sim 0.2$ nm^{-1}, which are related to the characteristic form factor and size of spherical scattering objects, practically do not shift within the C_p = 1.0−20.0 mg/mL range.

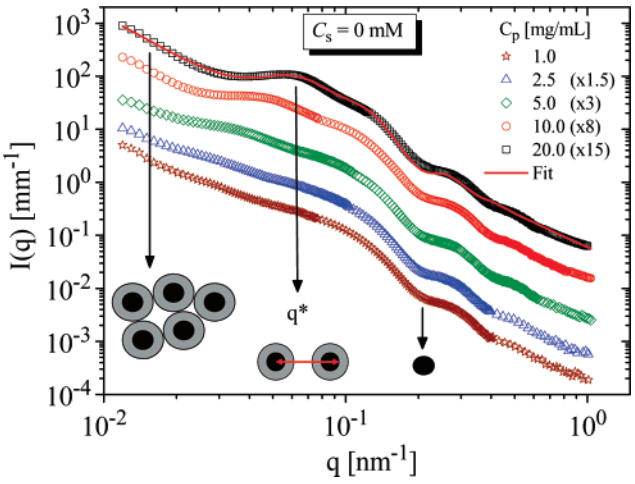

Figure 6. SAXS intensity profiles for PBuA$_{35}$-*b*-PECVPD$_{30}$ solutions at different copolymer concentrations (C_p) in the absence of salt. A cartoon showing the different structures observed in solution is also reported. The solid line indicates best fit to eq 8 for C_p = 20 mg/mL. For clarity, the SAXS patterns are rescaled by the factor indicated in the legend.

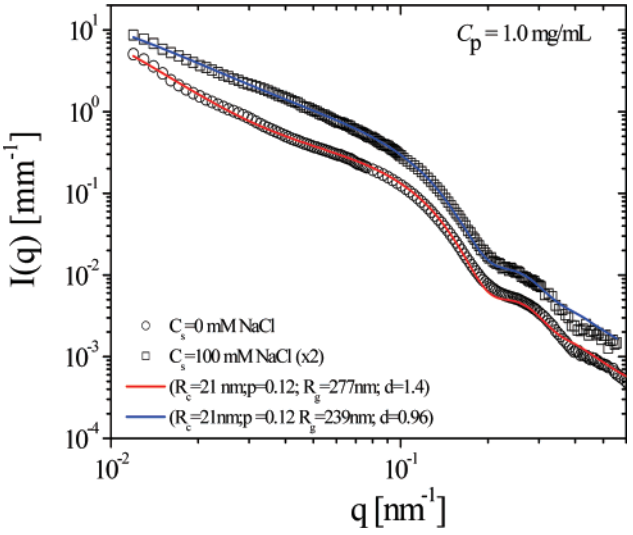

Figure 7. SAXS intensity profiles fitted using a polydisperse core−shell model (continuous lines) for spherical PBuA$_{35}$-*b*-PECVPD$_{30}$ micellar nanoparticles at C_p = 1.0 mg/mL in absence (open circles) and in presence of salt C_s = 100 mM (open squares). The parameters of the fits are also reported. For clarity, the data in presence of salt are rescaled by the factor indicated in the legend.

For C_p < 2.5 mg/mL, the SAXS intensity profiles can be fitted using eqs 3, 5, and 8 assuming $S(q) \approx 1$. Figure 7 shows the experimental SAXS data and fitting results (continuous lines) for spherical PBuA$_{35}$-*b*-PECVPD$_{30}$ micellar nanoparticles at C_p = 1.0 mg/mL in absence and in presence of C_s = 100 mM. In both cases, good agreement between experimental data and fitted curves is obtained. The resulting fit parameters revealed that changes in the ionic strength after micellization do not influence the core radius (R_c), which is essentially the same ($R_c \sim 21$ nm) in the absence of added salt (C_s = 0) and at high salt concentrations (C_s = 100 mM). Lack of significant changes in the micellar form factor upon addition of salt also revealed that the corona is nearly contrast matched with the solvent. The addition of salt causes a decrease in the aggregates (clusters) size from R_g = 277 nm at C_s = 0 down to R_g = 239 nm at C_s = 100 mM, as a result of electrostatic charge screening by counterions leading to less stretched (because of repulsive Coulomb forces) corona-forming segments. The limited q range

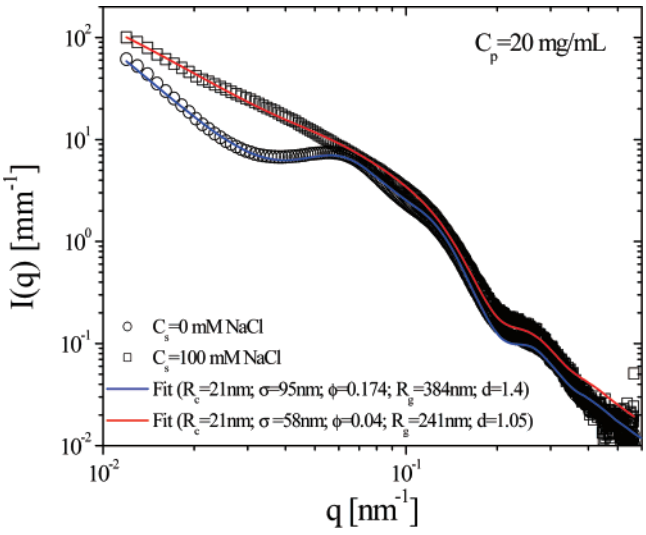

Figure 8. SAXS intensity profiles for PBuA$_{35}$-*b*-PECVPD$_{30}$ solutions at C_p = 20.0 mg/mL in absence (open squares) and in presence of salt C_s = 100 mM (open circles). The best fits to eq 8 are also shown. In the legend, the parameters of the fits are reported.

of the data excludes a precise determination of the radius of gyration of the clusters R_g and their fractal dimension d_f.

In Figure 8, the comparison between the two extreme conditions (minimal and high screening) is shown for C_p = 20 mg/mL (above c^*). The fits to eq 8 show a decrease of the effective diameter σ (which takes into account the contribution of hard core, the impenetrable shell, and the range of electrostatic interactions) from σ = 95 nm down to σ = 58 nm as consequence of the changes in the corona size and electrostatic interaction range with the addition of salt. The position of the minimum in the scattering patterns ($q \sim 0.2$ nm^{-1}) suggests that no changes are observed in the core size upon addition of salt. This result strongly suggests that N_{agg} is not affected by C_s. Moreover, it is very interesting to relate the changes in the effective volume fraction (from 0.17 to 0.04 as salt content increases from 0 up to 100 mM NaCl) with the decrease of R_H, reported in Figure 4 as a function of salt concentration. Knowing that $\varphi = N_pV$, we can attribute the changes in the effective volume fraction to partly the shrinking of the corona upon addition of salt [the value of 4.3 for the ratio between the volume fractions in absence and presence of salt as compared to the ratio between the effective hydrodynamic volumes, i.e., $(R_{H,C_s=0}/R_{H,C_s=100\ mM})^3 \sim 2.6$]. The remaining part can be attributed to the change in electrostatic interactions. Therefore, SAXS analyses correlate well with the DLS results, in spite of the fact that the salt effect seems to be more pronounced in the latter case.

Cryo-TEM Imaging Experiments. Cryogenic transmission electron microscopy analysis was performed on selected micellar solutions in order to verify the morphology of self-assembled structures. This technique is capable of imaging nanostructures in thin films of vitrified aqueous solutions, thus ideally preserving the sample characteristics in solution. The cryo-TEM images of PBuA$_{35}$-*b*-PECVPD$_{30}$ micelles in absence and in presence of added salt shown in Figure 9 confirm the spherical shape of the micelles obtained by SAXS (see also TEM micrograph in Figure S4 and low-magnification cryo-TEM micrographs in Figure S5). Because of the low contrast as in SAXS of the diffuse corona in water, only the core is seen in both cases, as previously reported for PBuA-*b*-PAA micelles[34] and PSS/PS lattices.[35] It is straightforwardly verified that the characteristic R_c is not affect by the ionic strength (R_c-TEM ≅

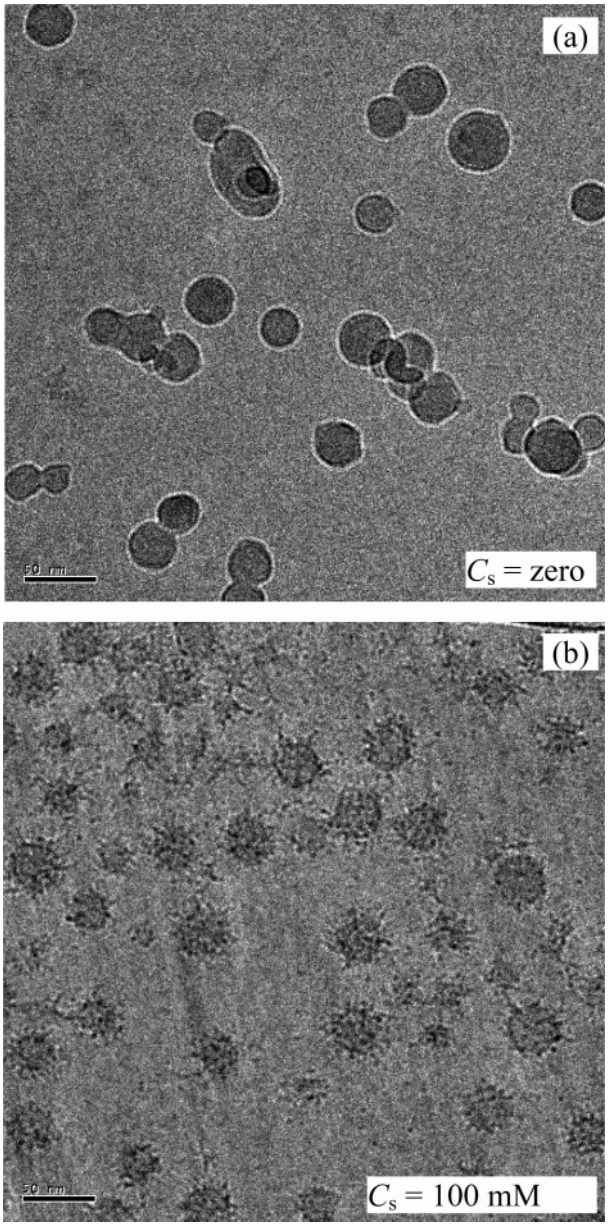

Figure 9. Cryo-TEM images of $PBuA_{35}$-*b*-$PECVPD_{30}$ micelles in absence (a) and in presence of salt $C_s = 100$ mM (b). The scale bar is 50 nm.

20 nm in Figure 9a,b), being entirely in agreement with findings discussed above (Figure 7). Micrographs taken in the presence of salt (Figure 9b) systematically revealed the presence of small dark points. Such an effect was previously observed by other authors[5,34,36] and is attributed to the salt-induced shrinking of corona chains into a few compact strands. Consequently, higher electron absorption areas (darker spots) are seen when the micelle image is projected in the plane.

Conclusions

The polyelectrolyte behavior of (PBuA-*b*-PECVPD) micelles was evidenced mainly by scattering techniques (DLS, SLS, and X-ray). Interesting pH-, salt-, and concentration-dependent polyelectrolyte features of this system in aqueous media is conferred by the hydrophilic PECVPD corona bearing negatively charged phosphonic diacid groups [$-P(O)(OH)_2$] with two distinct acid dissociation constants. The results clearly revealed that neither salt addition ($C_s = 0-100$ mM) nor polymer concentration ($C_p = 0.5-20$ mg/mL) affects the micelle core size. The analysis of the SAXS data shed a light on the micellar interactions and morphology in the absence and presence of added salt to the solution. A shrinking of the corona is observed upon addition of salt, whereas the size of core is invariant in all the range of concentrations and salt contents investigated. Moreover, the micelle corona thickness was significantly influenced by ionic strength and pH, with light scattering measurements demonstrating the existence of different regimes in the I_{sc} vs pH plots. Such a behavior was due to the increase in the negative charge density at the micellar corona as a consequence of deprotonation process of phosphonic diacid groups. Cryo-TEM images confirmed the spherical size of the aggregates.

Acknowledgment. R.B and A.R.B. acknowledge financial support from CNRS, Université Bordeaux 1, Région Aquitaine, European Union (EC grant FP6-NMP4-CT2003-505868 "Nanocues" to A.R.B.). V.S. and C.G. thank respectively CNPq and CAPES. The authors are grateful to Dr. F. Lecolley, Dr. J. Lai-Kee-Him, and N. Guidolin for their helpful discussions and contributions to this work. The European Synchrotron Radiation Facility is acknowledged for the provision of beam time.

Supporting Information Available: Molecular characteristics of the diblock copolymer, determination of its critical micelle concentration in water, titration data, a diagram of species distribution, and transmission electron microscopy images. This material is available free of charge via the Internet at http://pubs.acs.org.

References and Notes

(1) Ballauff, M.; Borisov, O. *Curr. Opin. Colloid Interface Sci.* **2006**, *11*, 316−323.
(2) Guenoun, P.; Muller, F.; Delsanti, M.; Auvray, L.; Chen, Y. J.; Mays, J. W.; Tirrell, M. *Phys. Rev. Lett.* **1998**, *81*, 3872−3875.
(3) Wittemann, A.; Ballauff, M. *Phys. Chem. Chem. Phys.* **2006**, *8*, 5269−5275.
(4) Zhou, F.; Huck, W. T. S. *Phys. Chem. Chem. Phys.* **2006**, *8*, 3815−3823.
(5) Förster, S.; Abetz, V.; Müller, A. H. E. *Adv. Polym. Sci.* **2004**, *166*, 173−210.
(6) Hales, K.; Pochan, D. J. *Curr. Opin. Colloid Interface Sci.* **2006**, *11*, 330−336.
(7) Borsali, R. In *Handbook of Polyelectrolytes and Their Applications*; Tripathy, S. K., Kumar, J., Nalwa, S., Eds.; American Scientific Publishers: Los Angeles, 2002; pp 249−265.
(8) Förster, S.; Schmidt, M. *Adv. Polym. Sci.* **1995**, *120*, 51−133.
(9) Muller, F.; Guenoun, P.; Delsanti, M.; Deme, B.; Auvray, L.; Yang, J.; Mays, J. W. *Eur. Phys. J. E* **2004**, *15*, 465−472.
(10) Romet-Lemonne, G.; Daillant, J.; Guenoun, P.; Yang, J.; Mays, J. W. *Phys. Rev. Lett.* **2004**, *93*, 148301−1−4.
(11) Roger, M.; Guenoun, P.; Muller, F.; Belloni, L.; Delsanti, M. *Eur. Phys. J. E* **2002**, *9*, 313−326.
(12) Forster, S.; Hermsdorf, N.; Bottcher, C.; Lindner, P. *Macromolecules* **2002**, *35*, 4096−4105.
(13) Norwood, D. P.; Benmouna, M.; Reed, W. F. *Macromolecules* **1996**, *29*, 4293−4304.
(14) Sorci, G. A.; Reed, W. F. *Macromolecules* **2002**, *35*, 5218−5227.
(15) Morfin, I.; Reed, W. F.; Rinaudo, M.; Borsali, R. *J. Phys. (Paris)* **1994**, *4*, 1001−1019.
(16) Schmidt, V.; Giacomelli, C.; Brisson, A.; Borsali, R. *Mater. Sci. Eng., C* **,** in press (DOI: 10.1016/j.msec.2007.04.025).
(17) Schmidt, V.; Giacomelli, C.; Lecolley, F.; Lai-Kee-Him, J.; Brisson, A. R.; Borsali, R. *J. Am. Chem. Soc.* **2006**, *128*, 9010−9011.
(18) Huang, J.; Matyjaszewski, K. *Macromolecules* **2005**, *38*, 3577−3583.
(19) Pecora, R.; Berne, B. J. *Dynamic Light Scattering With Applications to Chemistry, Biology and Physics;* Dover Publications: Mineola, NY, 2000.
(20) Provencher, S. W. *Makromol. Chem.* **1979**, *180*, 201−209.
(21) Narayanan, T.; Diat, O.; Boesecke, P. *Nucl. Instrum. Methods A* **2001**, *467*, 1005−1009.

(22) Kotlarchyk, M.; Chen, S.-H. *J. Chem. Phys.* **1983**, *79*, 2461−2469.
(23) Sztucki, M.; Narayanan, T. *J. Appl. Crystallogr.* **2007**, *40*, s459−s462.
(24) Brumberger, H. In *Modern Aspects of Small Angle Scattering*; Kluwer Academic: Dordrecht, 1995.
(25) Colombani, O.; Ruppel, M.; Schubert, F.; Zettl, H.; Pergushov, D. V.; Muller, A. H. E. *Macromolecules* **2007**, 4338−4350.
(26) Kalyanasundaran, K.; Thomas, J. K. *J. Am. Chem. Soc.* **1977**, *99*, 2039−2044.
(27) Li, X.; Reed, W. F. *J. Chem. Phys.* **1991**, *94*, 4568−4580.
(28) Moinard, D.; Borsali, R.; Taton, D.; Gnanou, Y. *Macromolecules* **2005**, *38*, 7105−7120.
(29) Korobko, A. V.; Jesse, W.; Lapp, A.; Egelhaaf, S. U.; van der Maarel, J. R. C. *J. Chem. Phys.* **2005**, *122*, 024902−1−11.
(30) Hariharan, R.; Biver, C.; Russel, W. B. *Macromolecules* **1998**, *31*, 7514−7518.
(31) Muller, F.; Romet-Lemonne, G.; Delsanti, M.; Mays, J. W.; Daillant, J.; Guenoun, P. *J. Phys.: Condens. Matter* **2005**, *17*, S3355−S3361.
(32) Guenoun, P.; Davis, H. T.; Tirrell, M.; Mays, J. W. *Macromolecules* **1996**, *29*, 3965−3969.
(33) Korobko, A. V.; Jesse, W.; Egelhaaf, S. U.; Lapp, A.; van der Maarel, J. R. C. *Phys. Rev. Lett.* **2004**, *93*, 177801-1−177801-4.
(34) Colombani, O.; Ruppel, M.; Burkhardt, M.; Drechsler, M.; Schumacher, M.; Gradzielski, M.; Schweins, R.; Muller, A. H. E. *Macromolecules* **2007**, *40*, 4351−4362.
(35) Samokhina, L.; Schrinner, M.; Ballauff, M.; Drechsler, M. *Langmuir* **2007**, *23*, 3615−3619.
(36) Erhardt, R.; Zhang, M.; Boker, A.; Zettl, H.; Abetz, C.; Frederik, P.; Krausch, G.; Abetz, V.; Muller, A. H. E. *J. Am. Chem. Soc.* **2003**, *125*, 3260−3267.

MA702182P